Estuarine, Coastal and Shelf Science (1999), **48,** 439–450
Article No. ecss.1998.0432 , available online at http://www.idealibrary.com on IDEAL®

The Influence of Sediment Load on Tidal Dynamics, a Case Study: Cádiz Bay

O. Alvarez[a], A. Izquierdo[a], B. Tejedor[a], R. Mañanes[a], L. Tejedor[a] and B. A. Kagan[a,b]

[a]*Departamento de Fisica Aplicada, Universidad de Cádiz, Apdo 40, 11510, Puerto Real (Cádiz), Spain*
[b]*Shirshov Institute of Oceanology, Russian Academy of Sciences, St. Petersburg Branch, 30 Pervaya Liniya, 199053, St. Petersburg, Russia*

Received 26 June 1998 and accepted in revised form 29 October 1998

A two-dimensional, non-linear, finite-difference, hydrodynamic model was applied to Cádiz Bay to study the influence of sediment load on tidal dynamics. The sediment load effect is represented parametrically as a dependence of the drag coefficient on the relative settling velocity (the ratio of the settling velocity of suspended particles to the bottom friction velocity) and the relative friction velocity (the ratio of the bottom friction velocity to its critical value at which sediment particles begin to go into suspension). This dependence is derived from a solution of the equations describing the vertical structure of the sediment-stratified bottom logarithmic layer. A comparison of the model predictions with and without allowance for the sediment load effect shows that the latter is responsible for small local changes of the amplitude and phase of tidal elevation and the maximum depth-averaged tidal velocity, the result counting in favour of the conventional approach whereby the influence of sediment load on tidal dynamics is considered to be negligible. However, it is apparent after close inspection of the model predictions that the sediment load effect tends to enhance the time-space variability of the tidal characteristics. In particular, it results in an increase in the maximum depth-averaged velocity and a decrease in the drag coefficient for the periods of flood and ebb currents, thus reducing the shear bottom stress and the tidal energy dissipation by about half.

Keywords: tidal dynamics; energetics; suspended particles; parameterization; Cádiz Bay

Introduction

At present, there is a hierarchy of coupled hydrodynamic/suspended sediment transport models intended for describing tidal dynamics and sediment transport processes in shallow waters. It involves two-dimensional, depth-integrated models (e.g. Lin *et al.*, 1986; De Vriend, 1987; Falconer, 1992; Lin & Falconer, 1994), two-dimensional (in a vertical plane) models (e.g. Van Rijn, 1986; Celik & Rodi, 1988), quasi-three-dimensional models based on specifying the vertical profiles of mean velocity and suspended sediment concentration (e.g. Van Rijn, 1984; Galapatti & Vreugdenhil, 1985; Falconer & Owens, 1990; Lou & Ridd, 1997) and three-dimensional models (e.g. Koutitas & O'Connor, 1980; Miller, 1984; O'Connor & Nicholson, 1988; Cahyono, 1993).

In all these models, except the model of Van Rijn (1984), suspended sediment particles are considered as being passive and thereby not affecting flow dynamics. The consequences of this assumption are obvious: if the change-over of sediment particles into suspension is determined by the processes of erosion at the bed and entrainment at the upper boundary of the bed-load layer, while the vertical distribution of suspended particles is governed by the processes of turbulent diffusion and gravitational settling, then for non-equilibrium situations a steady, horizontally homogeneous, sediment-bearing turbulent flow can be only stably stratified. In this case, other conditions being the same, the intensity of turbulence will be smaller and the mean velocity will be greater than their values in clear-water flow due to the expenditure of turbulent kinetic energy in overcoming the buoyancy force.

The above qualitative conclusions are supported by observational evidence (e.g. Smith, 1977; Smith & McLean, 1977). For instance, as demonstrated in Lin and Falconer (1995), a spring tide at the Halton Middle site in the Humber Estuary, the north-east coast of England, is marked by a sudden increase in suspended sediment concentration and its accompanied strengthening of tidal velocity. Moreover, both these events are found to be unpredictable with a coupled hydrodynamic/suspended sediment

0272–7714/99/040439+12 $30.00/0

transport model in which the influence of sediment load on tidal dynamics is disregarded.

The simplest way of taking into account this influence is to employ a three-dimensional model complimented by a turbulent kinetic energy closure scheme with a proper description of the suspended sediment stratification effect. However, such a model is expensive to apply. The questions arise: How to take into account the influence of sediment load on tidal dynamics without resort to solving the problem on the vertical structure of a sediment-stratified turbulent flow in each specific case? And, generally, how significant is this influence?

As has been shown by Kagan *et al.* (1998), the suspended sediment stratification effect may be allowed for in terms of a ' variable ' von Karman's constant provided it is understood that its variability is apparent and that a ' variable ' von Karman's constant is nothing more than a convenient means for parameterization of the influence of sediment load on flow dynamics. Note that the dependence of von Karman's constant on suspended sediment concentration has been examinated empirically, with the aid of measured velocity and concentration profiles, by Karim (1981), Wang (1981) and Van Rijn (1984). Clearly, their dependencies, like the more recent dependence obtained in a similar manner by Nough (1989), do not offer versatility even when eliminating the errors associated with the existence of the wake-flow region (see Coleman, 1981). In contrast to these empirically based dependencies, a functional dependence for von Karman's constant put forward by Kagan *et al.* (1998) starts from a solution to the problem of the vertical structure of the sediment-stratified bottom logarithmic layer. In the present paper, the solution is employed to specify the drag coefficient as a function of the external parameters determining the vertical structure of the sediment-stratified bottom logarithmic layer. This theoretically based dependence is incorporated into a two-dimensional, non-linear, finite-difference, hydrodynamic model to clarify the influence of sediment load on the tidal dynamics of Cádiz Bay and thus to provide answers to the above questions.

The paper is organized as follows. The next section discusses briefly a k–l model for the vertical structure of the sediment stratified bottom logarithmic layer, which serves as the basis for parameterization of the sediment load effect. The model differs from other models of this type in accounting for a dependence of the mixing length on the Kolmogorov number (analogous to the flux Richardson number in sediment-bearing turbulent flow) and some dependences of the height of the bed-load layer and the reference suspended sediment concentration at this height on the excess shear bottom stress. Also presented here is a parameterization of the sediment load effect, represented as a dependence of the drag coefficient on the two dimensionless parameters (relative settling velocity and relative friction velocity) that, apart from the dimensionless height, determine uniquely the vertical structure of the sediment stratified bottom logarithmic layer. In the penultimate section, the simulation results for the M_2 constituent in Cádiz Bay are given with and without allowance for the sediment load effect. Comparison of these results offers a clearer view of where and when, if at all, this effect shows up most clearly. A discussion in the final section completes this paper.

' Variable ' von Karman's constant and the drag coefficient

We shall consider the sediment stratified bottom logarithmic layer (SSBLL). The timescale for this layer is defined as the ratio of its height to the friction velocity amplitude (the latter is a suitable velocity scale for the bottom boundary layer in tidal flow). If the characteristic height of the bottom logarithmic layer and the characteristic friction velocity amplitude in shallow waters are taken as being equal, respectively, to 10 m and 1 cm s^{-1} (Bowden, 1978), then the timescale is 15 min, implying that it is smaller than the period of any one of the tidal constituents. This is a plausible justification for the condition of quasi-steadiness and, hence, for the existence of the logarithmic vertical profile of mean velocity in the near-bottom layer of tidal flow.

To describe the vertical structure of the quasi-steady, horizontally homogenous SSBLL for non-equilibrium situations we make use of a k–l turbulence model. In addition, we assume that the mixing length l is a function of the height z above the seabed and the Kolmogorov number Ko characterizing the ratio of expenditures of turbulent kinetic energy for overcoming the buoyancy force to shear production of turbulent kinetic energy in sediment stratified turbulent flows. Also, we speculate that the reference level identified with a height of the upper boundary of the bed-load layer and the reference suspended sediment concentration at this height are functions of the excess shear bottom stress. Then, on rearranging and introducing dimensionless variables, the initial set of equations and boundary conditions may be written as (Kagan *et al.*, 1995)

$$\frac{dv}{dy} = \frac{1}{\Phi(Ko)(1-Ko)^{1/4}}, \qquad (1)$$

$$\frac{ds}{dy}=\frac{-\alpha_c w_s/\kappa u_\star}{\Phi(Ko)(1-Ko)^{1/4}}, \tag{2}$$

$$Ko=a_0\gamma_1\kappa^2\left(\frac{w_s}{\kappa u_\star}\right)\left(\frac{u_\star}{u_{\star c}}\right)^2\left[1-\left(\frac{u_{\star c}}{u_\star}\right)^2\right]^2\Phi(Ko)$$
$$(1-Ko)^{1/4}\exp(y+s), \tag{3}$$

$$v-v_a=0,\quad s=0,\quad \text{at}\quad y=0, \tag{4}$$

where $v=(\kappa/u_\star)u$ is the dimensionless mean velocity; v_a is its value at the upper boundary of the bed-load layer; $s=\ln(c/c_a)$ is the dimensionless suspended sediment concentration; $y=\ln(z/z_a)$ is the dimensionless height; $u_\star$ and $u_{\star c}$ are the friction velocity and its critical value at which sediment particles begin to go into suspension; c and c_a are the suspended sediment concentration and its value at $z=z_a$, respectively; w_s is the settling velocity of suspended particles; $\Phi(Ko)$ is a certain non-increasing function of its argument; α_c is the turbulent Schmidt number, being a function of Ko; κ is von Karman's constant.

Following Smith and McLean (1977) we define the bed-load layer height z_a and the suspended sediment concentration c_a at this height which appear in the definitions of y and s as

$$z_a=a_0(u_\star^2/g')[1-(u_\star/u_{\star c})^2];$$

$$c_a=\gamma_1(u_\star/u_{\star c})^2[1-(u_{\star c}/u_\star)^2]; \tag{5}$$

where $g'=g(\rho_s-\rho)/\rho$ is the reduced gravity; ρ_s and ρ are the densities of suspended material and water, respectively; $a_0=26{\cdot}3$ and $\gamma_1=1{\cdot}56{\cdot}10^{-3}$ are numerical constants.

As known, a wide variety of relationships exists in the literature to predict z_a and c_a. Carrying out a detailed comparison of seven relationships against a common set of experimental data, García and Parker (1991) showed that the relationships given by Smith and McLean (1977) and Van Rijn (1984) performed best. That is why we accept the expressions (5) as the definitions of z_a and c_a. Besides, it is known that the functions $\Phi(Ko)$ and $\alpha(Ko)$ are not defined within the framework of the semi-empirical theory of turbulence. Because of this, their specification calls for further comments. It would appear reasonable that $\Phi(Ko)\to 1$ at $Ko\to 0$ and $\Phi(Ko)\to 0$ at $Ko\to Ko_c$, where $Ko_c\approx 0{\cdot}20$ is the critical value of Ko. The former of these conditions means that, as the suspended sediment concentration reduces to zero, the mixing length tends to its value in clear-water flow, whereas the latter means that small-scale turbulence degenerates when the Kolmogorov number reaches its critical value. With allowance made for these considerations, the function $\Phi(Ko)$ may be specified as

$$\Phi(Ko)=(1-Ko/Ko_c) \tag{6}$$

Clearly, this approximation is rather crude. It is not applicable for coarse suspended particles with linear sizes exceeding the Kolmogorov length microscale at which turbulent kinetic energy dissipation occurs. It is also not applicable for particles with neutral buoyancy and for particles whose concentrations, even if these particles have negative buoyancy, are kept constant in the vertical direction. In both of these cases, the expenditure of turbulent kinetic energy for overcoming the buoyancy force is lacking. Let this also be so for the case where the particle velocity disturbances responsible for the fluid velocity fluctuations with lengthscales of the order of the Kolmogorov length microscale and, hence, additional losses of turbulent kinetic energy due to dissipation are ignored. Then from the turbulent kinetic energy budget equation supplemented with the Kolmogorov's similarity relationships for the eddy viscosity and the turbulent kinetic energy dissipation as well as expression (6), it follows that all the characteristics of the turbulence will remain the same as in clear-water flow. This, however, is inconsistent with the data from laboratory measurements (Yalin, 1972; Kulick *et al.*, 1994) and the results of numerical simulations of particle interactions with wall turbulence (Pan & Banerjee, 1996). Despite these limitations, expression (6) is a useful alternative to the traditionally accepted hypothesis for complete similarity of the mixing length in the kolmogorov number, the hypothesis equivalent to replacing $\Phi(Ko)$ by 1.

As regards the turbulent Schmidt number α_c, its dependence on Ko has not been firmly established as yet. In particular, some experimental studies (e.g. Jobson & Sayre, 1970) suggest that $\alpha_c=1{\cdot}0$. Other studies, such as those of Karim (1981) and Celik (1983), show that lower values of α_c are in the range of 0·5 to 1·0. There are in addition empirical formulae relating α_c to $w_s/u_\star$ (Van Rijn, 1984; Whitehouse, 1995; Kawanishi & Yokosi, 1997) and to suspended sediment concentration (Lees, 1991; Kawanishi & Yokosi, 1997). In the present paper we use the relationship

$$\alpha_c=\alpha_c^N(1-a_1^{-1}Ko)/(1-a_2^{-1}Ko),\quad Ko<Ko_c, \tag{7}$$

which has been accepted in second-order turbulence closure models (Mellor & Yamada, 1974, 1982). Here, $a_1=0{\cdot}245$ and $a_2=0{\cdot}233$ are numerical constants; $\alpha_c^N=1{\cdot}0$ is the turbulent Schmidt number for neutral stratification ($Ko=0$).

Now, when the formulation of the problem may be considered as complete, we call attention to the fact

that the solution of Equations (1)–(7) is uniquely determinated by the three dimensionless parameters: the Rouse number $w_s/\kappa u_\star$, the relative friction velocity $u_\star/u_{\star_c}$ and the dimensionless height y (or $g'z/u_\star^2$ if one takes into account the definition of z_a; see Equation (5)). Such a solution has been obtained by Kagan *et al.*, (1995) for the bounded domain $0{\cdot}2 \le w_s/\kappa u_\star \le 2{\cdot}5$, $2{\cdot}0 \le u_\star/u_{\star_c} \le 10{\cdot}0$, $0{\cdot}5 \le y \le 6{\cdot}0$ of the parametric space $\{w_s/\kappa u_\star,\ u_\star/u_{\star_c},\ y\}$. From this solution, von Karman's constant κ can be found by approximating the vertical profiles $v(y)$ at different points of the parametric plane $(w_s/\kappa u_\star,\ u_\star/u_{\star_c})$ with straight lines and by determining the associated values of the derivative dv/dy. Thereupon the resulting set of discrete values of κ is approximated by a polynomial giving an analytical expression for the dependence $\kappa = \kappa(w_s/\kappa u_\star,\ u_\star/u_{\star_c})$. The latter, on rearrangement, yields an algebraic equation for von Karman's constant κ as a function of the relative settling velocity $w_s/u_\star$ and the relative friction velocity $u_\star/u_{\star_c}$, which with a real non-negative solution in the range for 0·1 to 1·0 for $w_s/u_\star$ and from 2·0 to 10·0 for $u_\star/u_{\star_c}$ can be closely approximated by

$$\kappa = 0{\cdot}4 + 0{\cdot}0755 \ln\left[\frac{w_s/u_\star}{\tanh(0{\cdot}6(u_\star/u_{\star_c} - 1))}\right] - 0{\cdot}0004(u_\star/u_{\star_c} - 1) \qquad (8)$$

if $\kappa \le 0{\cdot}4$; otherwise, $\kappa = 0{\cdot}4$

It is worth noting once more that the functional dependence (8) is merely a reflection of changes of the mean velocity profile produced by varying suspended sediment stratification at different values of the external parameters that determine the vertical structure of the SSBLL. In this sense it must be regarded only as a proper tool for parameterizing the influence of sediment load on flow dynamics.

In terms of a ' variable ' von Karman's constant, the drag coefficient in the quadratic resistance law for bottom friction is defined as

$$C_D = (\kappa/\kappa_0)^2 C_{D0} \qquad (9)$$

where κ_0 and C_{D0} are reference values of κ and C_D.

Application to Cádiz Bay

Cádiz Bay is near latitude 36·5°N on the south-west coast of Spain (Figure 1). It faces west to the Gulf of Cádiz and is landlocked around its south-western, southern and eastern margins by the mainland. The bay is subdivided into two basins, a shallower one (Inner Bay) and a deeper one (Outer Bay), connected

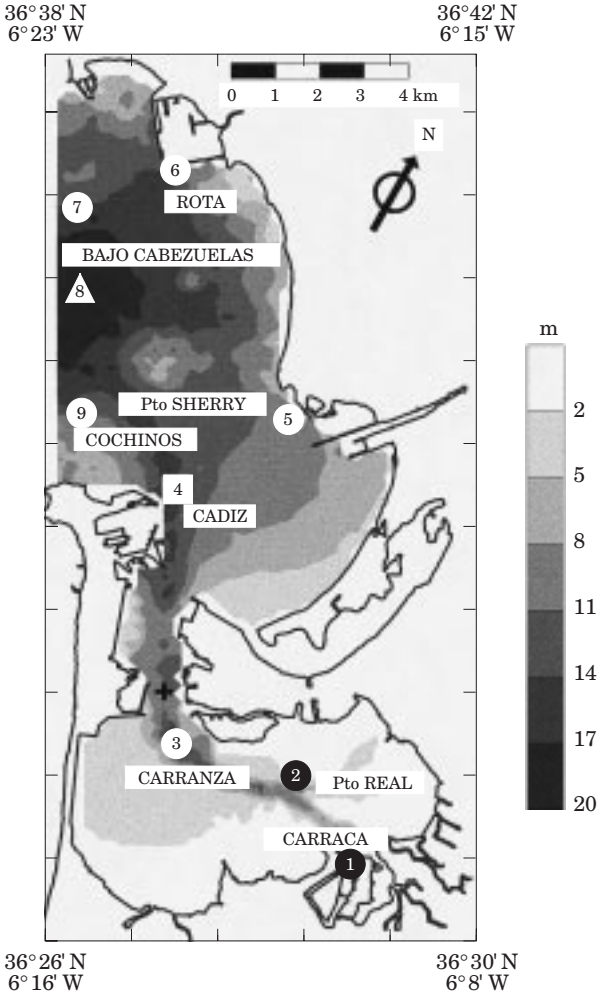

FIGURE 1. Map of Cádiz Bay superimposed on the bathymetry. Also shown are the locations of the tide-gauge, bottom pressure and current meter measurements referred to in the text. The location of the tide gauge is denoted by the square, the locations of the bottom pressure sensors are denoted by open and closed circles and the location of current meter mooring is denoted by the triangle. The position of the a point referred to in the text is indicated by the cross.

together by the narrow Puntales Channel. The bay is shallow, with a maximum depth of 20 m at its seaward edge, and is characterized by dominantly semidiurnal co-oscillating tides with amplitudes of ~1 m for M_2 constituent and ~0·4 m for the S_2 constituent. Seabed sediments consist mainly of coarse silt with the median grain-size of ~40 μm in Inner Bay and of medium sand with the median grain-size of ~190 μm in Outer Bay. Quartz grains comprise 85% of all the sediments (Gutiérrez *et al.*, 1996).

During February 1997, a one month field study of the tides in Cádiz Bay was carried out. The locations of the tide gauge and bottom pressure measurements are shown in Figure 1. The tidal elevation at one tide

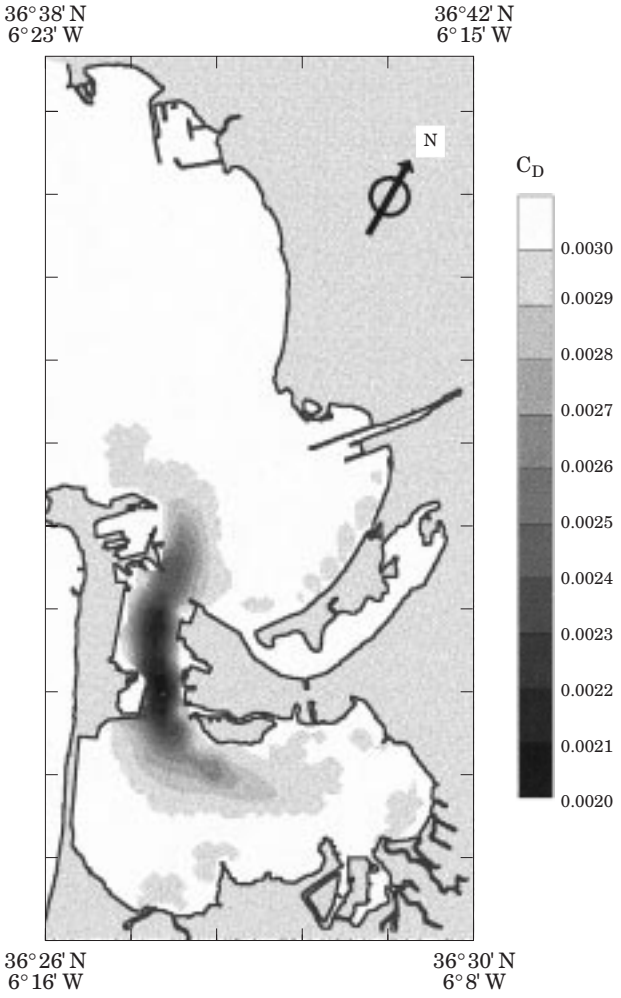

FIGURE 2. Mean (over a tidal cycle) drag coefficient predicted with allowance for the sediment load effect.

gauge location and seven bottom pressure sensor locations in the bay were recorded using, respectively, OTT Thales and Anderaa WLR7 tidal gauges. Due to strong shipping traffic, current meter measurements were only possible at 1 location at the open boundary. These were made with the moored Anderaa DCM12 current meter deployed at a depth of 14 m. The location of the current meter mooring is also shown in Figure 1. Standard harmonic analyses (Godin, 1972) verified by inference calculations (Foreman & Henry, 1989), were performed on the tidal elevation, current velocity and bottom pressure data to evaluate the amplitudes and phases for each of the resolvable tidal constituents.

The two-dimensional, non-linear, finite-difference, hydrodynamic model developed by Alvarez *et al.* (1997) was applied to simulate the spatial distributions of tidal elevation, tidal current ellipse parameters and tidal energy budget characteristics for the M_2 constituent in Cádiz Bay. A free slip condition was set at the coastal boundary. At the open boundary, a radiation condition written in terms of the deviations of tidal elevation and velocity from their observed values was employed to ensure that, when disturbances were generated, they all propagated away from the model domain. The observed values of tidal characteristics with this boundary condition were evaluated as follows: the tidal elevations along the open boundary were obtained by using a linear interpolation/extrapolation of those derived from the bottom pressure observations at stations Cochinos and Bajo de Cabezuelas, while the tidal velocities were taken as being equal to the M_2 velocity derived from the measurement data at the current meter mooring location. The bathymetry shown in Figure 1 was derived from the IHM chart number 443.

The model calculations were performed with and without allowance for the sediment load effect which was parameterized as described previously. For the solution to be smooth the equations of motion were supplemented with smoothing terms. The latter were defined by a horizontal eddy diffusion operator acting on tidal velocity throughout the model domain except for its boundaries. The horizontal eddy viscosity coefficient was chosen so that it would be as small as possible and, at the same time, be capable of suppressing short wavelength disturbances in the field of tidal characteristics. Both these requirements were met with a horizontal eddy viscosity coefficient value of 15 $m^2 s^{-1}$. As was apparent after performing the appropriate numerical experiments, the use of this value rather than a smaller value of the horizontal eddy viscosity coefficient did not affect considerably the accuracy of the model predictions. Specifically, with the horizontal eddy viscosity coefficient taken as 15, 10 and 1 $m^2 s^{-1}$, the rms errors in the predicted values of tidal elevation amplitudes and phases were 0·86 cm and 1·32°, 0·83 cm and 1·44° and 0·83 cm and 1·72°, respectively.

The settling velocity and the critical friction velocity were found as functions of grain size from the appropriate empirical curves presented by Soulsby and Wainwright (1987). Because of the lack of measurement data, the mean grain size of suspended particles was prescribed more or less arbitrarily to be 50 μm in the belief that it would fall in the range of the observed values of sea-bed grain size (also see below). The values of the other constants were taken $\kappa_0 = 0{\cdot}4$, $C_{D0} = 0{\cdot}003$ and $g' = 15{\cdot}6$ m s^{-2}.

The tidal dynamics equations were integrated on a Arakawa C staggered grid using a semi-implicit Crank-Nicolson scheme. A spatial resolution of

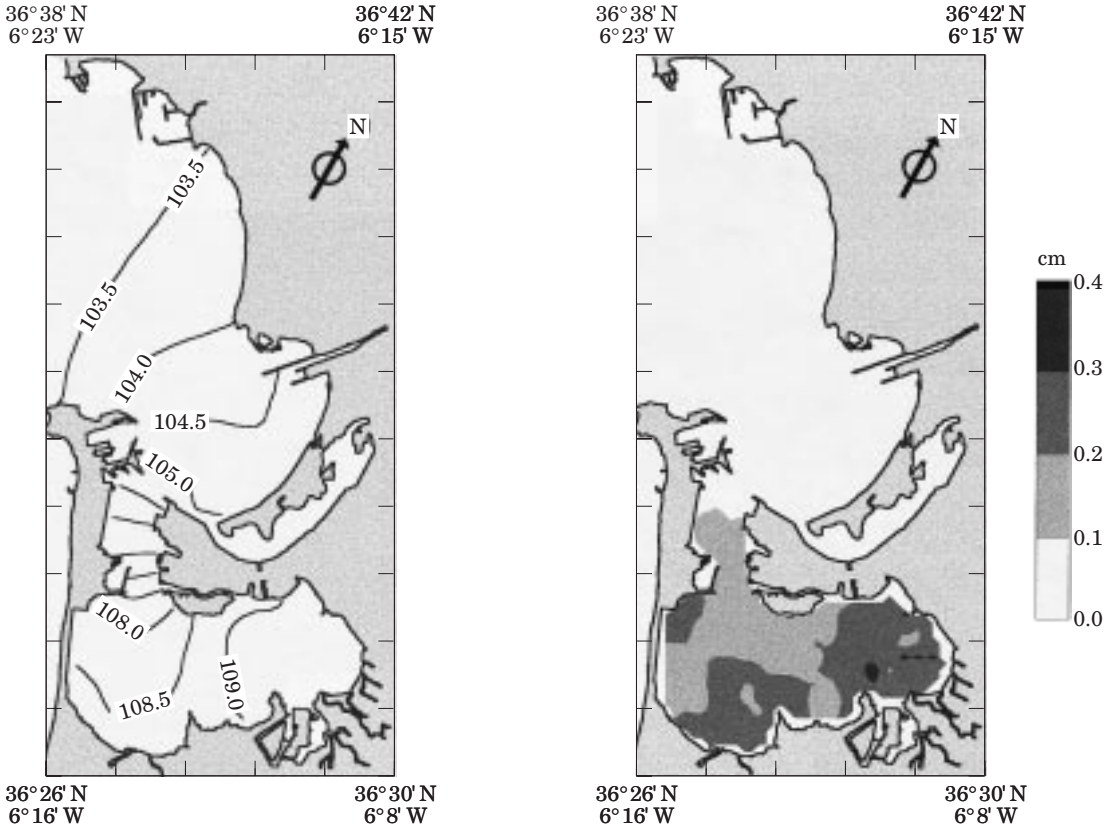

FIGURE 3. Chart of isoamplitudes, in centimetres, for the M_2 constituent (left) and the difference between the amplitude values predicted with and without allowance for the sediment load effect (right).

210 m and a time step of 30 s were chosen. The model was run for eight tidal cycles to achieve a stable time-periodic solution. After establishing this solution, the model run was continued for one more tidal period so that the amplitudes and phases of tidal elevation and velocity as well as the mean tidal energy budget characteristics and their changes in time over the tidal cycle could be determined. Thereafter the cotidal chart and the maps of tidal current ellipse parameters and mean tidal energy budget characteristics for the M_2 constituent were constructed.

The modelling results are presented in Figures 2–7. Also shown here are the differences between the model predictions with and without allowance for the sediment load effect. As can be seen, the differences for the amplitude and phase of tidal elevation and the maximum depth-averaged tidal velocity (Figures 3–5) are small compared to local values of these characteristics being, at least for tidal elevation, within the accuracy of the model predictions (see Table 1). However the differences are not small compared to the spatial changes of these characteristics within the domain considered. In fact, judging from Figures 3 and 4, the maximum differences for the amplitude and phase of tidal elevation amount to 0·4 cm and 0·7°, while their spatial changes are not more than 5·5 cm and 3·5°, respectively. In other words, the influence of sediment load on the tidal dynamics of Cádiz Bay shows up most vividly in the spatial variability of the amplitudes and phases of tidal elevation and velocity. This is also true for the mean (over a tidal cycle) energy budget characteristics with a single reserve: in a given case, not only the spatial variability but also the mere values of the mean tidal energy budget characteristics are markedly changed due to the sediment load effect. As an illustration, we draw attention to the differences for the mean tidal energy flux (Figure 6) and the mean rate of tidal energy dissipation (Figure 7) in the regions adjacent to Puntales Channel where small-scale eddies in the mean tidal energy flux field occur. Here, the differences can be of the same order of magnitude as the values of the characteristics *per se*.

An analysis of the variability of the above tidal characteristics during a tidal cycle shows that the differences are more than just mentioned. So, for example, at the point marked in Figure 1 by the cross

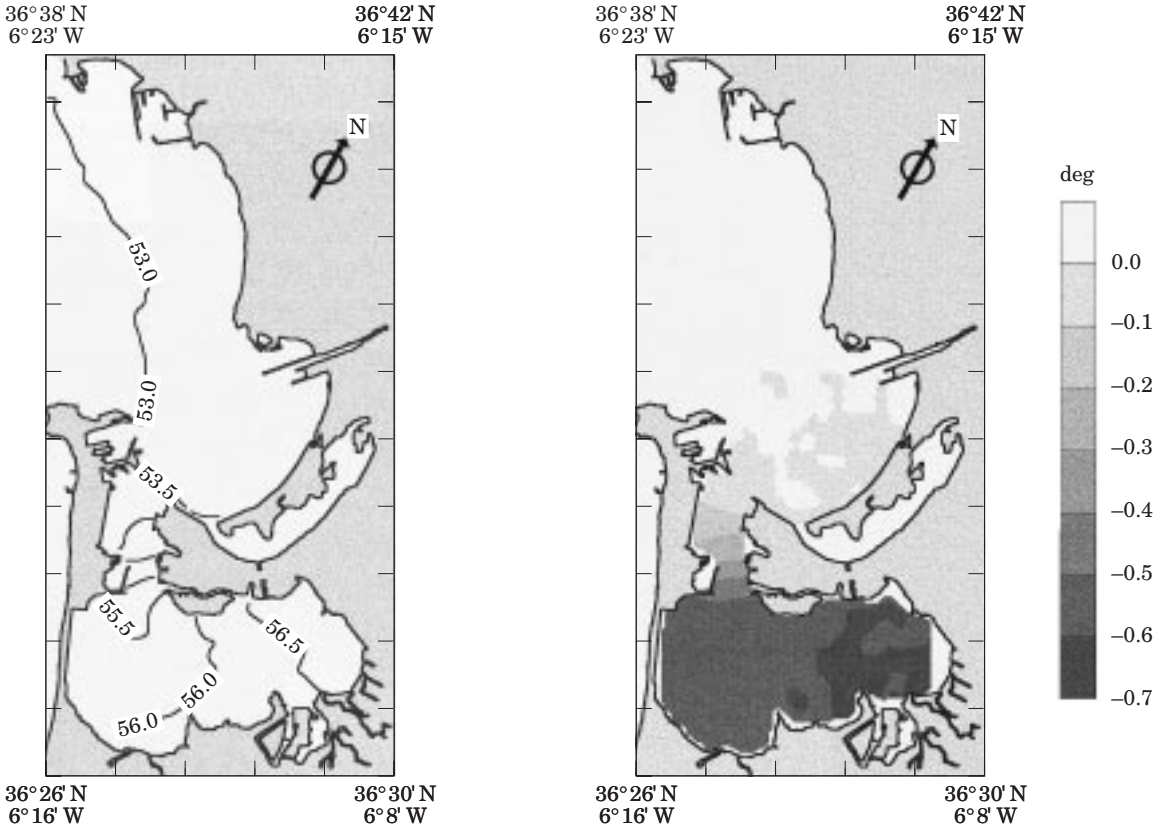

FIGURE 4. Chart of isophases, in degrees, for the M_2 constituent (left) and the difference between the phase values predicted with and without allowance for the sediment load effect (right).

the differences between the values of maximum tidal velocity predicted with and without allowance for the sediment load effect may be as much as $2{\cdot}8\ \mathrm{cm\ s^{-1}}$ for flood current and $1{\cdot}5\ \mathrm{cm\ s^{-1}}$ for ebb current. Also, this effect causes the drag coefficient to vary from 0·003 to 0·0012. As a result, the shear bottom stress and the tidal energy dissipation are reduced by about half; more precisely, their values are $0{\cdot}61\ \mathrm{Nm^{-2}}$ and $0{\cdot}43\ \mathrm{Wm^{-2}}$ at the time instant of maximum flood current and $0{\cdot}54\ \mathrm{Nm^{-2}}$ and $0{\cdot}38\ \mathrm{Wm^{-2}}$ at the time instant of maximum ebb current, whereas with no sediment load these are $1{\cdot}46\ \mathrm{Nm^{-2}}$ and $1{\cdot}00\ \mathrm{Wm^{-1}}$ in the first case and $1{\cdot}21\ \mathrm{Nm^{-2}}$ and $0{\cdot}80\ \mathrm{Wm^{-2}}$ in the second. By comparing these differences with those inherent in the amplitude and phase of tidal elevation and the maximum depth-averaged tidal velocity, we get the conclusion that local changes of these characteristics may be not proper indicators of the sediment load effect.

As has already been intimated, the solution under discussion was obtained assigning an arbitrary value of 50 μm for the mean suspension particle grain size. It is therefore desirable to clarify how sensitive the solution is to variations in this value. To this end, the model was run with the mean suspension particle grain size taken as 40 and 190 μm, the observed values of the median sea-bed sediment grain size in the region of interest. The resulting values of the differences between the time-independent tidal characteristics predicted with and with no sediment load, together with those appropriate to the previously accepted value of 50 μm for the mean suspension particle grain size, are listed in Table 2. The data of this table suggests that the changes in the differences due to variations in grain size are commensurable with the values of the differences as such. The same can be said of the variability of the tidal characteristics during a tidal cycle. In fact, if the mean suspension particle grain size is taken as 40 μm, the differences between the values of maximum tidal velocity, shear bottom stress, tidal energy flux per unit length and tidal energy dissipation predicted with and with no sediment load are, respectively, $2{\cdot}9\ \mathrm{cm\ s^{-1}}$, $-0{\cdot}87\ \mathrm{N\ m^{-2}}$, $-0{\cdot}90\ \mathrm{Kw\ m^{-1}}$ and $-0{\cdot}58\ \mathrm{W\ m^{-2}}$ at the time instant of maximum flood current and $1{\cdot}3\ \mathrm{cm\ s^{-1}}$, $-0{\cdot}71\ \mathrm{N\ m^{-2}}$, $-0{\cdot}55\ \mathrm{Kw\ m^{-1}}$ and $-0{\cdot}44\ \mathrm{W\ m^{-2}}$ at the time instant of maximum ebb current. Alternatively, if the mean suspension

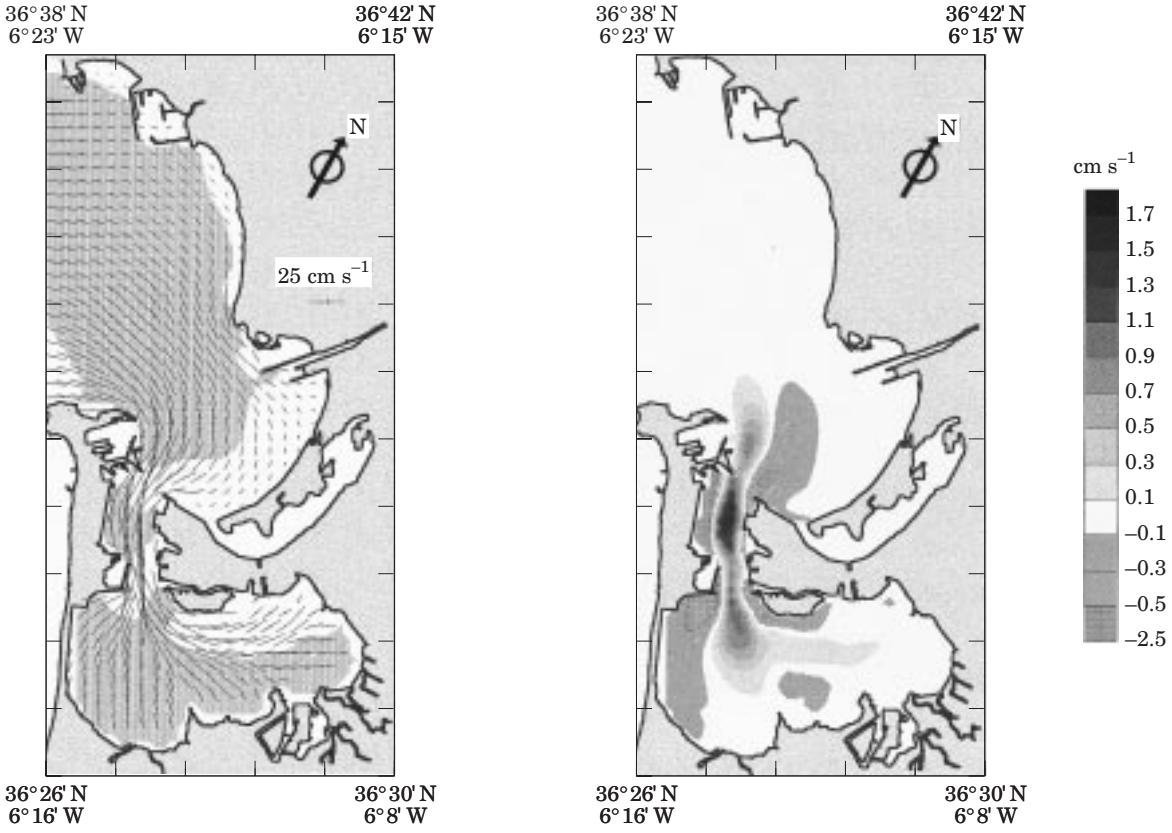

FIGURE 5. Major and minor axes of tidal ellipses and sense of rotation of tidal velocities for the M_2 constituent (left) and the difference between the maximum velocity values predicted with and without allowance for the sediment load effect (right). Shaded and unshaded regions correspond to clockwise and anticlockwise rotation, respectively.

particle grain size is taken as 190 μm, these are $0{\cdot}5\ \mathrm{cm\,s^{-1}}$, $-0{\cdot}17\ \mathrm{Nm^{-1}}$, $-0{\cdot}045\ \mathrm{Kwm^{-1}}$ and $-0{\cdot}11\ \mathrm{W\,m^{-2}}$ at the time instant of maximum flood current and $0{\cdot}3\ \mathrm{cm\,s^{-1}}$, $-0{\cdot}15\ \mathrm{N\,m^{-2}}$ $-0{\cdot}034\ \mathrm{Kwm^{-1}}$ and $-0{\cdot}10\ \mathrm{Wm^{-2}}$ at the time instant of maximum ebb current. Clearly, the mere changes in the tidal characteristics due to the sediment load effect are quite sensitive to variations in grain size and thus the sediment load-induced changes in the tidal dynamics and energetics of Cádiz Bay which are depicted in Figures 2–7 should be recognized as tentative.

Discussion

In the existing practice of modelling tides in shallow waters, the influence of sediment load on tidal dynamics is usually disregarded without proof. We have tried to quantify this influence so as to clarify whether the above simplification is acceptable. For this purpose, a simple parameterization of the sediment load effect has been incorporated into a two-dimensional, non-linear, finite-difference, hydrodynamic model and the modified model has been applied to Cádiz Bay to simulate the spatial distributions of tidal elevation, tidal ellipse parameters and tidal energy budget characteristics for the M_2 constituent, as well as the changes produced by the effect in question. The parameterization of this effect is based on a solution of the equations for the sediment stratified bottom logarithmic layer (SSBLL) under non-equilibrium conditions and represented as a dependence of the drag coefficient on the two dimensionless parameters that, apart from the dimensionless height, determine uniquely the vertical structure of the SSBLL. These dimensionless parameters are the relative settling velocity (the ratio of the settling velocity of suspended particles to the bottom friction velocity) and the relative friction velocity (the ratio of the bottom friction velocity to its critical value at which sediment particles begin to go into suspension). Cádiz Bay was chosen to evaluate the significance of the sediment load effect for two reasons: first, the bay is typical of other shallow basins where silt and sand suspended sediments discharged from seabed erosion are transported and dispersed to offshore deep waters;

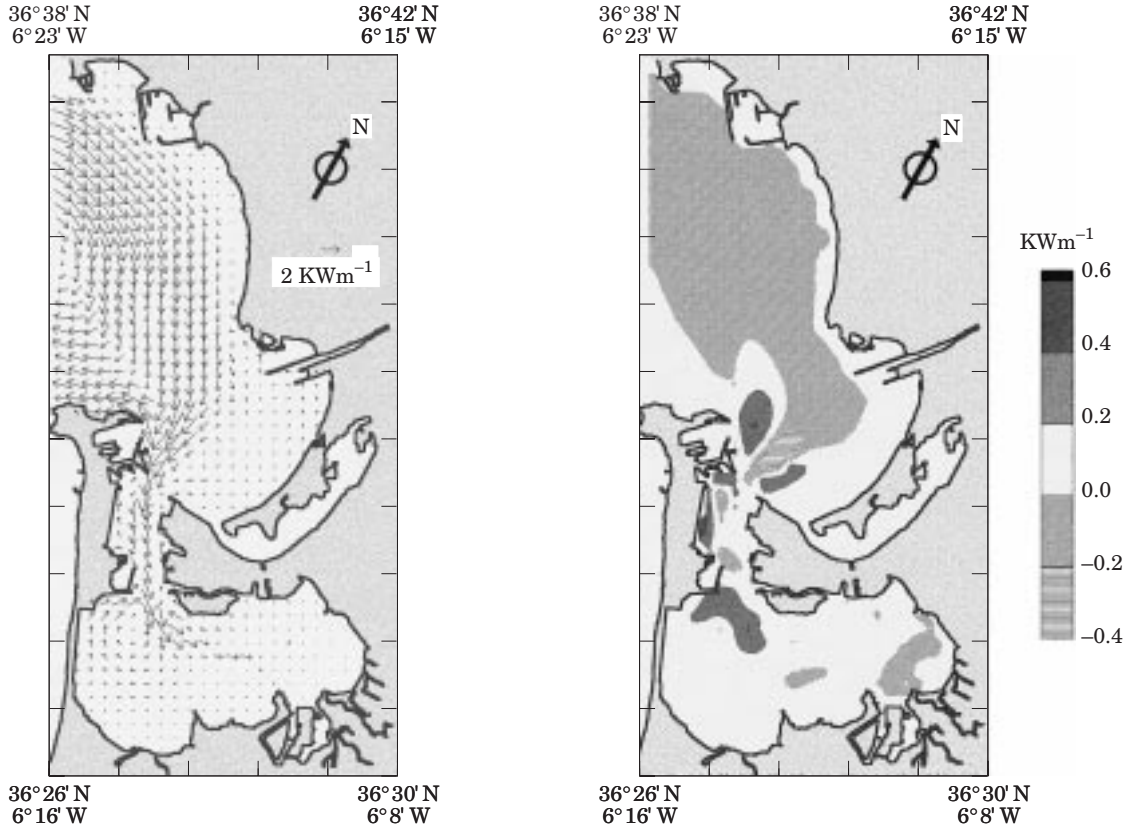

FIGURE 6. Mean (over a tidal cycle) tidal energy flux per unit length for the M_2 constituent (left) and the difference between the flux values predicted with and without allowance for the sediment load effect (right).

second, an extensive experimental programme for the study of tides had been carried out in the bay, which makes it possible to test model predictions.

When the model predictions for tidal elevation are compared with the tide-gauge and bottom pressure data obtained in the framework of this programme, it has been found that their correspondence is reasonable but not as good as that reported in other shallow water tidal modelling investigations. There are certain reasons for this. One is the abandonment of tuning model parameters, in particular, the drag coefficient and the horizontal eddy viscosity coefficient, to fit predictions to experimental data. For instance, almost perfect agreement between the predicted tidal elevations and the available measurement data in Cádiz Bay may be obtained with the above coefficients taken as 0·004 and 30 $m^2\,s^{-1}$, respectively. Clearly, such a way, even though it is justified in practical applications, only masks an inadequacy regarding the knowledge of the physical processes responsible for the formation of tides and is thus unacceptable in studies of these processes as such.

Another reason is associated with prescribing a constant reference drag coefficient. Normally, this coefficient is identified with the drag coefficient for neutral suspended sediment stratification, which is determined by the height above the bottom and a bottom roughness length. The latter, in turn, is determined by the entire spectrum of roughness elements over the area with a linear scale of the order of the bottom logarithmic layer height. Because the required information about the spatial distribution of roughness elements is usually lacking, any allowance for the variability in the reference drag coefficient within the region of interest becomes impossible. With no tuning model parameters, this results in inevitable discrepancies between the predicted and observed values of tidal characteristics.

One more reason for such discrepancies is the conventional use of the depth-averaged tidal velocity $\overline{\mathbf{u}}$ instead of the local tidal velocity $\mathbf{u}_1$ at a fixed height z_l within the bottom logarithmic layer as a quantity specifying the shear bottom stress. A rough estimate of the error due to replacing $\mathbf{u}_1$ by $\overline{\mathbf{u}}$ may be obtained as follows: if one assumes that the vertical distribution of tidal velocity in shallow waters is described by the logarithmic law and that sense of rotation of tidal velocity remains unaltered within the bottom

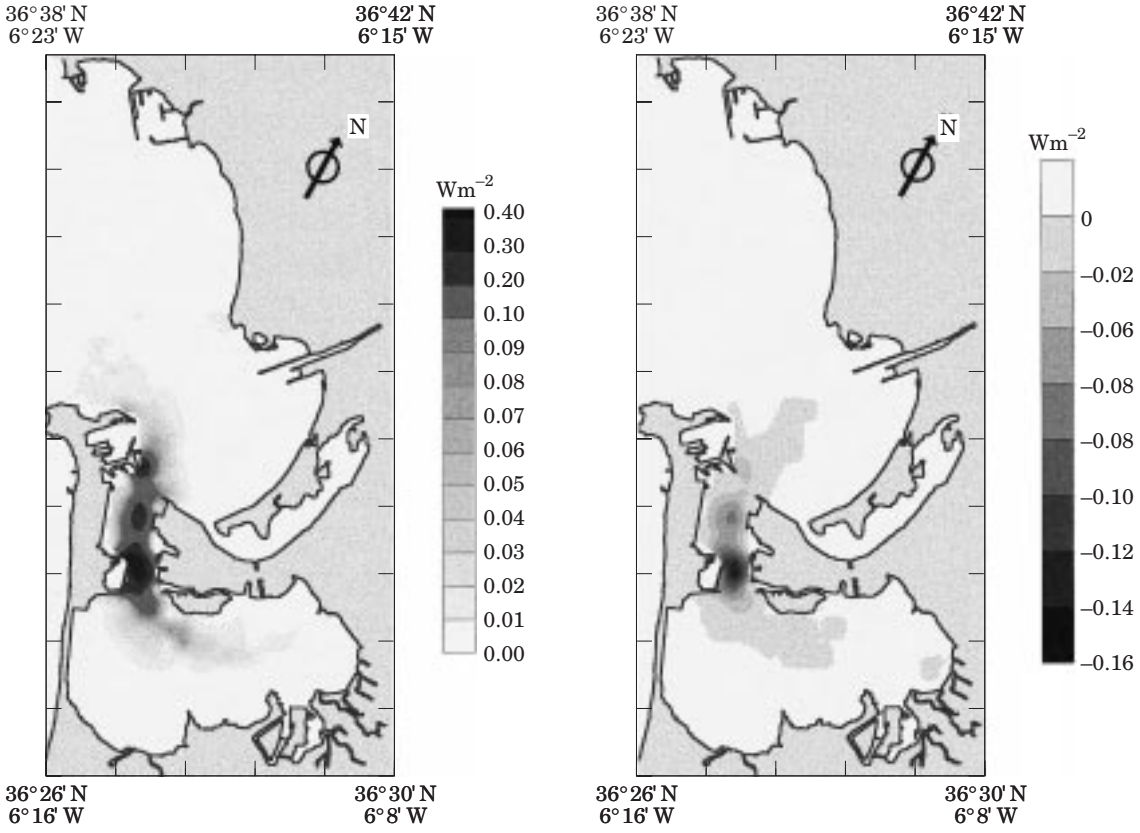

FIGURE 7. Same as Figure 6, but for tidal energy dissipation.

TABLE 1. Predicted and observed tidal constants (the M_2 constituent) at the locations of tide-gauge and bottom pressure measurements

	Amplitude (cm)		Phase (deg.)	
Station	Observed	Predicted	Observed	Predicted
CARRACA (1)	108·0	109·2	60·0	56·3
PTO. REAL (2)	106·5	109·0	57·9	56·6
P. CARRANZA (3)	107·2	107·3	57·7	55·2
PTO. CADIZ (4)	103·1	104·6	55·0	53·0
PTO. SHERRY (5)	103·2	104·0	52·6	53·2
ROTA (6)	101·4	103·3	53·8	53·1

logarithmic layer, then the shear bottom stresses, specified by $\bar{\mathbf{u}}$ and $\mathbf{u}_1$ will differ from each other by the factor $|\bar{\mathbf{u}}|^2/|\mathbf{u}_1| \approx \ln^2(h/2{\cdot}73z_0)\ln^{-2}(z_1/z_0)$, where h is the depth; z_0 is the bottom roughness length. The magnitude of this factor is greater than one at $h>2{\cdot}73z_1$ and smaller than one at $h<2{\cdot}73z_1$. Hence, the use of the depth-averaged tidal velocity instead of the local one can give rise to an overestimation of the shear bottom stress at relatively great depths and its underestimation at small depths. In the case of Cádiz Bay where the bottom roughness length takes the value 0·22 cm (it corresponds to silty sand deposits, see Heathershaw, 1979), the shear bottom stress may be overestimated at $z_1=1$ m by the factor 1·5. Finally, other discrepancies may occur as a result of neglecting the phase difference between the shear bottom stress and the depth-averaged velocity (Marchuk & Kagan, 1977; Lavell & Mofjeld, 1983). With these caveats in mind, the observed agreement between the predicted and observed tidal constants in Cádiz Bay is better than had been expected.

TABLE 2. Differences between the model predictions with and with no sediment load at the selected point in the Puntales Channel for various values of mean suspended sediment particle grain size

Characteristics	Mean suspension particle grain size		
	40 μm	50 μm	190 μm
Amplitude of tidal elevation (cm)	0·3	0·2	0·1
Phase of tidal elevation (deg.)	− 0·4	− 0·3	0·0
Major semiaxis of tidal velocity (cm s^{-1})	0·9	0·9	0·2
Phase of maximum tidal velocity (deg.)	0·5	0·4	0·0
Mean drag coefficient (10^{-3})	− 1·14	− 1·03	− 0·15
Mean tidal energy flux per unit length (Kw m^{-1})	− 0·003	0·010	0·017
Mean tidal energy dissipation (W m^{-2})	− 0·19	− 0·18	− 0·03

As has been shown from a comparison of the model predictions with and without allowance for the sediment load effect, it is responsible for small local changes of the amplitude and phase of tidal elevation and the maximum depth-averaged tidal velocity for the M_2 constituent in Cádiz Bay. This bay is not exceptional in that the changes reflecting the influence of sediment load on tidal dynamics are less pronounced there than somewhere else. Therefore it is plausible that similar small changes of tidal characteristics have to be typical of other not-too-shallow bays and estuaries. At first glance this inference seems contradictory to equations (8) and (9) from which it follows that under variations of the relative settling velocity from 0·1 to 1·0 and of the relative friction velocity from 2·0 to 10·0, the variations that are almost ubiquitous in shallow waters, the sediment load effect tends to decrease the drag coefficiently 2–3 times. The contradiction is resolved as follows: the drag coefficient varies markedly only for a short time when the bottom friction velocity is at (or close to) its maximum value, while during the rest of the tidal cycle the drag coefficient does not differ too much from its reference value. That is why the local values of the mean (over a tidal cycle) drag coefficient and tidal energy budget characteristics, like the local values of the amplitude and phase of tidal elevation and the maximum depth-averaged tidal velocity, which are presented in Figures 2–7, do not differ as much as expected from their values predicted with no sediment load.

This, in turn, means that the conventional approach ignoring the influence of sediment load on two-dimensional tidal dynamics is justified for the amplitudes and phases of tidal elevation and depth-averaged tidal velocity at not-too-small depths and weak or moderately strong tidal currents like those that occur in Cádiz Bay. Also, major manifestations of the sediment load effect should be searched for either in the time-space variability of tidal characteristics predicted by two-dimensional models or in this variability and the vertical structure of tidal flow predicted by three-dimensional models rather than in local changes of tidal elevation and velocity. Clearly, the problem being discussed is worthy of more attention than has been given to it previously.

Acknowledgements

The work was carried out during a stay of B. A. Kagan as visiting professor at University of Cádiz. The authors would like to thank Dr A. D. Heathershaw for both his valuable suggestions and his help regarding our use of English which has helped to improve this paper. The work was partially supported by the INTAS Programme in the framework of the Project 96-1875 and by the CYTMAR Project MAR95-1896-C02-02.

References

Alvarez, O., Tejedor, B. & Tejedor, L. 1997 Simulación hidrodinámica en el área de la Bahía de Cádiz. Análisis de las constituyentes principales. *IV Jornadas Españolas de Ingeniería de Puertos y Costas*. Servicio de Publicaciones de la Unsiversidad Politécnica de Valencia-98.2125, 125–136.

Bowden, K. F. 1978 Physical problems of the benthic boundary layer. *Geophysical Surveys* **3,** 255–296.

Cahyono, A. 1993 Three dimensional numerical modelling of sediment transport processes in non-stratified estuarine and coastal waters. Ph.D. Thesis, Department of Civil Engineering, University of Bradford, Bradford, 315 pp.

Celik, I. 1983 Numerical modelling of sediment transport in open channel flows. In *Mechanics of Sediment Transport* (Sümer, B. H. & Müller, A., eds). A. A. Balkema Publishers, Rotterdam, The Netherlands, 173–181.

Celik, I. & Rodi, W. 1988 Modelling suspended sediment transport in non-equilibrium situations. *Journal of Hydraulic Engineering* **114,** 1157–1191.

Coleman, N. L. 1981 Velocity profiles with suspended sediment. *Journal of Hydraulic Research* **19,** 211–229.

De Vriend, H. J. 1987 2DH mathematical modelling of morphological evolutions in shallow water. *Coastal Engineering* **11,** 1–27.

Falconer, R. A. 1992 Flow and water quality modelling in coastals and island waters. *Journal of Hydraulic Research* **30,** 437–452.

Falconer, R. A. & Owens, P. H. 1990 Numerical modelling of suspended sediment fluxes in estuarine waters. *Estuarine, Coastal and Shelf Science* **31,** 745–762.

Foreman, M. G. G. & Henry, R. F. 1989 The harmonic analysis of tidal model time series. *Advances in Water Resources* **12,** 109–120.

Galappatti, G. & Vreugdenhil, C. B. 1985 A depth-integrated model for suspended sediment transport. *Journal of Hydraulic Research* **23,** 359–375.

García, M. & Parker, G. 1991 Entrainment of bed sediment into suspension. *Journal of Hydraulic Engineering* **117,** 414–435.

Gutierrez, J. M., Achab, M., Parrado, J. M. *et al*. 1996 Distribution of recent facies at the bottom of the Bay of Cádiz. *Geogaceta* **21,** 155–157.

Godin, G. 1972 *The Analysis of Tides*. University of Toronto Press, Toronto, Ontario, Canada, 264 pp.

Heathershaw, A. D. 1979 The turbulent structure of the bottom boundary layer in a tidal current. *Geophysical Journal of the Royal Astronomical Society* **58,** 395–430.

Jobson, H. E. & Sayre, W. W. 1970 Vertical transfer in open channel flow. *Journal of Hydraulic Engineering* **96,** 703–724.

Kagan, B. A., Schrimpf, W. & Eifler, W. 1995 Universal structure of the sediment-stratified bottom logarithmic layer. *Physics and Chemistry of the Earth* **20,** 141–148.

Kagan, B. A., Schrimpf, W. & Utkin, K. B. 1998 Parameterization of the sediment stratification effect on flow dynamics. *Annales Geophysicae, Supplement IV to Volume* **16,** C 1108.

Karim, Ud. F. 1981 Computer-based predictors for sediment discharge and friction factor of alluvial streams. Ph.D. Thesis, University of Iowa, Iowa City, Iowa.

Kawanishi, K. & Yokosi, S. 1997 Characteristics of suspended sediment and turbulence in a tidal boundary layer. *Continental Shelf Research* **17,** 359–375.

Koutitas, C. & O'Connor, B. A. 1980 Numerical modelling of suspended sediments. *Advances in Water Resources* **3,** 51–57.

Kulick, J. D., Fessler, J. R. & Eaton, J. K. 1994 Particle response and turbulence modification in fully developed channel flow. *Journal of Fluid Mechanics* **277,** 109–134.

Lavell, J. M. & Mofjeld, H. D. 1983 Effects of time-varying viscosity on oscillatory turbulent channel flow. *Journal of Geophysical Research* **88,** 7607–7616.

Lees, B. J. 1991 Relationship between eddy viscosity of seawater and eddy diffusivity of suspended particles. *Geo-Marine Letter* **1,** 249–254.

Lin, B. & Falconer, R. A. 1995 Modelling sediment fluxes in estuarine waters using a curvilinear coordinate grid system. *Estuarine, Coastal and Shelf Science* **43,** 413–428.

Lin, P. N., Han, Z. C. & Sun, H. B. 1986 Two-D simulation of sediment transport and bed deformation by tides. Proceedings of the Third International Symposium on River Sedimentation, University of Mississippi, U.S.A., 388–399.

Lou, J. & Ridd, P. V. 1997 Modelling of suspended sediment transport in coastal areas under waves and currents. *Estuarine, Coastal and Shelf Science* **45,** 1–16.

Marchuk, G. I. & Kagan, B. A. 1977 *Ocean Tides*. Gidrometeoizdat, Leningrad, 295 pp. (in Russian); Pergamon Press, Oxford 1984 (in English).

Mellor, G. L. & Yamada, T. 1974 A hierarchy of turbulent closure models for planetary boundary layers. *Journal of Atmospheric Sciences* **31,** 1791–1806.

Mellor, G. L. & Yamada, T. 1982 Development of a turbulence closure models for geophysical fluid problems. *Review of Geophysics* **20,** 851–875.

Miller, H. P. 1984 Three-dimensional free surface suspended particles transport in the South Biscayne Bay, Florida. *International Journal of Numerical Methods in Fluids* **4,** 901–914.

Nough, N. 1989 The Von Karman coefficient in sediment laden flow. *Journal of Hydraulic Research* **27,** 477–499.

O'Connor, B. A. & Nicholson, J. 1988 A three-dimensional model of suspended particulate sediment transport. *Coastal Engineering* **12,** 157–174.

Pan, Y. & Banerjee, S. 1996 Numerical simulation of particle interactions with turbulence. *Physics of Fluids* **8,** 2733–2755.

Smith, J. D. 1977 Modelling of sediment transport on continental shelves. In *The Sea: Ideas and Observations on Progress in the Study of the Seas* (Goldberg, E. D., ed.). Vol. 6, John Wiley and Sons, Inc. 539–557.

Smith, J. D. & McLean, S. R. 1977 Spatially averaged flow over a wavy surface. *Journal of Geophysical Research* **82,** 1725–1746.

Soulsby, R. L. & Wainwright, B. L. S. A. 1987 A criterion for the effect of suspended sediment on near-bottom velocity profiles. *Journal of Hydraulic Research* **25,** 341–355.

Van Rijn, L. C. 1984 Sediment transport. Part 2: Suspended load transport. *Journal of Hydraulic Engineering* **110,** 1613–1641.

Van Rijn, L. C. 1986 Mathematical modelling of suspended sediment in non-uniform flows. *Journal of Hydraulic Engineering* **112,** 433–455.

Wang, S. 1981 Variation of Karman constant in sediment-laden flow. *Journal of the Hydraulic Division, Proceedings of the American Society of Civil Engineers* **107,** 407–417.

Whitehouse, R. 1995 Observations of the boundary layer characteristics and the suspension of sand at a tidal site. *Continental Shelf Research* **15,** 1549–1567.

Yalin, M. S. 1972 *Mechanics of Sediment Transport*. Pergamon Press, Inc., New York, 290 pp.